SAR Simulation Report

Model No: A2140

FCC ID: BCGA2140

Date of Simulation:
05/10/2020-08/10/2020
Location:
Apple Inc., Cupertino, CA, USA

Table of Contents

1 Introduction

The magnetic charger described in this document inductively charge other wireless charging devices.

The charging function operates at 127.7kHz (Qi) and 360.0kHz. The charger supports charging at 5W, 7.5W and 15W power and NFC tag operation. The charger doesn't have any internal battery.

2 Wireless Power Transfer System

The wireless power transfer system consists of a transmitting coil with 11 turns and measures 7.5 uH nominally in free air. The receiver coil consists of 13 turns and measures 9.06 uH nominally in free air. Both coils are wound spirally.

Below are key parameters of the design that will be helpful in determining worst-case use for exposure:

Item	**Description**
Max Power Delivered	15 W (delivered at rectifier)
Full Charge Time	3 hours 10 minutes (from empty)
Operating Frequency	f_0 = 360 kHz
Communications/Modulation Method	ASK for Phone to Charger (load modulation) FSK for Charger to Phone
Object Detection Mode	Low Power Pulse

Below is the charging profile/sequence. Maximum power transfer of 15 W takes place only when the battery is near empty.

Battery State of Charge	Charge Duration in min	Power Delivered to rectifier in Watts
0-12%	11	15 W
12-50%	30	Changes between 2.5 and 13 W
50-100%	120	Changes between 2 and 6 W

3 SAR Simulations Methodology

The following steps are taken to show the validity of the model used for SAR Simulations:

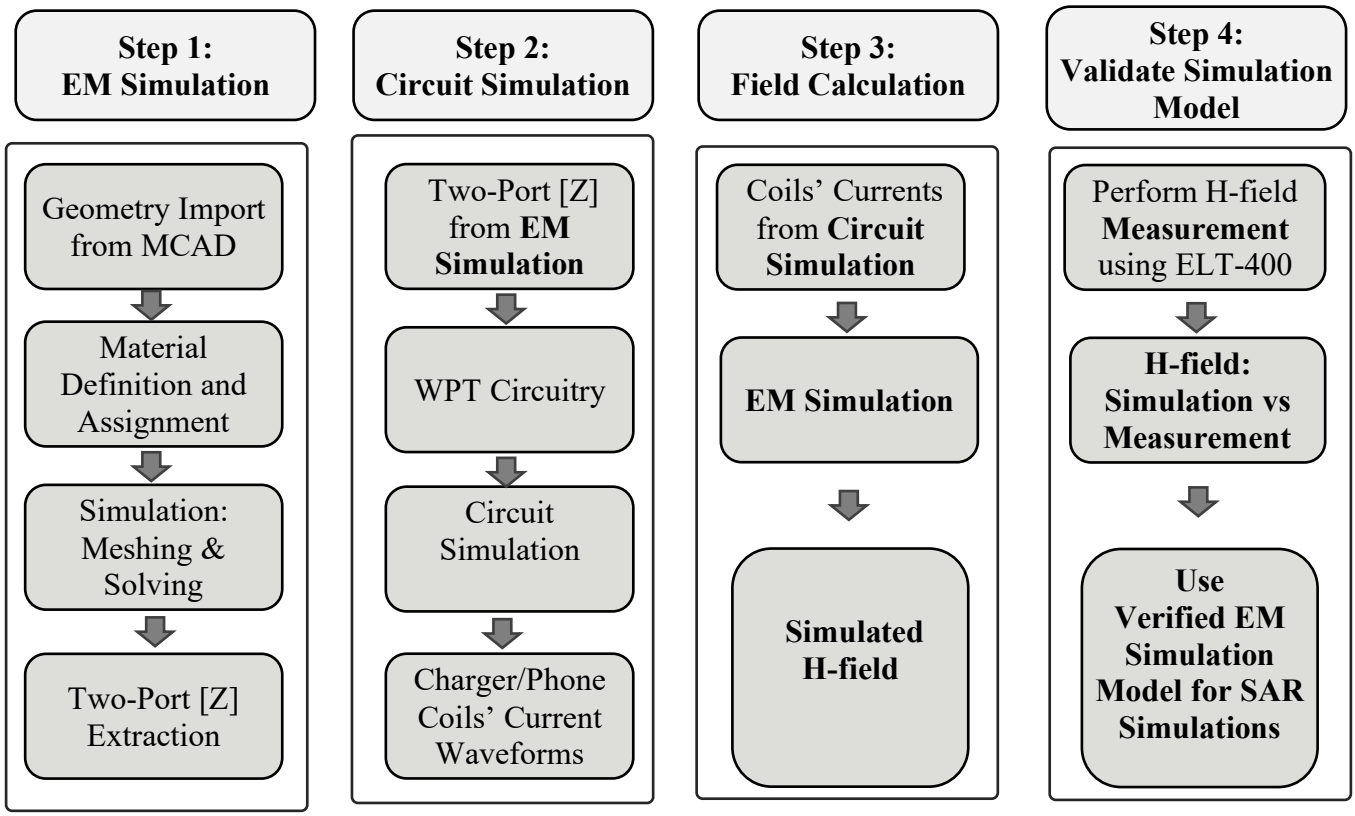

1) EM Simulation:
    a. Import a CAD model that represents the actual product in the simulation tool.
    b. Define material properties inside the product based on vendor's inputs.
    c. Extract two-port network impedance matrix ([Z]) from the simulation.
2) Circuit Simulation:
    a. Include the impedance matrix in the wireless power transfer (WPT) circuit model.
    b. Run circuit simulation and extract coils' current waveforms.
3) Field, H-field, and SAR Calculations:
    a. Use the current waveforms to drive the EM simulation model.
    b. Calculate H-field from simulation.
    c. Compare simulated H-field with measured H-field
    d. Once a correlation is established, this model will be used for SAR simulations.

4 H-field Measurements

A Narda ELT-400 probe is used to measure the H-field above the DUT. Below is a picture of the probe, an x-ray image of the probe, and the measurement setup. The probe has three orthogonal loops with radius of 10 mm. These loops are used to measure H-field in different directions. The distance from the DUT to the probe is 0 mm. However, the loops are covered with a plastic shell of 6 mm thickness. Therefore, the distance from the center of the probe to the DUT is 16 mm. These factors have been considered in simulation of the H-field.

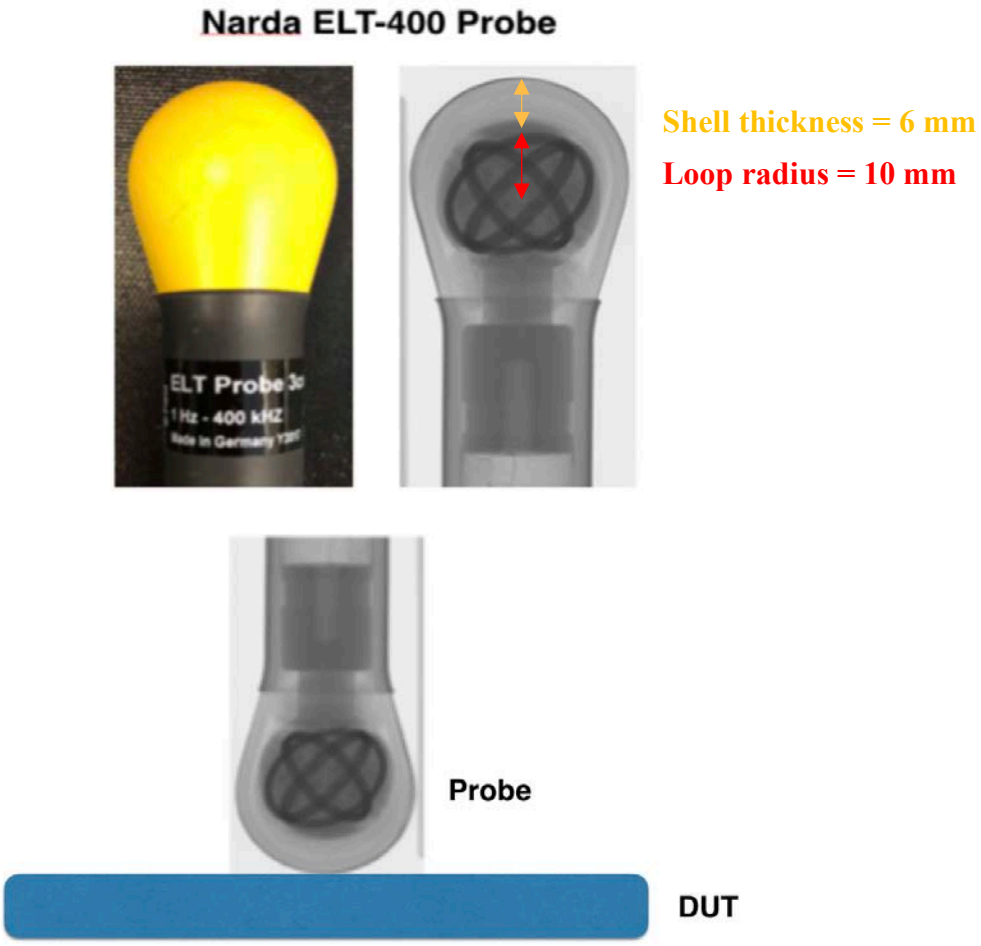

5 H-field Simulations

The electromagnetics simulations are conducted using commercially available software ANSYS HFSS. In order to validate the simulation model, H-field measurements are made on the DUT (as explained above) and compared to the simulated model results. The validated model is then used for SAR simulations.

For the simulations, following Step 1 described above, the CAD file that represents the DUT is first imported. Then the proper material properties are assigned at the operating frequency. After the simulation is completed, the two-port network [Z] was extracted and used with the WPT circuit model. This WPT model includes the charger source as well as the charging client side rectifier circuit. Solving the circuit using ANSYS Circuit tool, the proper excitation per transmitter (charger) and receiver (phone) coils are calculated. Later, these current waveforms are fed into the ANSYS HFSS to excite the coils and create H-field.

As shown below, the phone and charger can be unintentionally forced by user to be laterally misaligned or vertically separated.

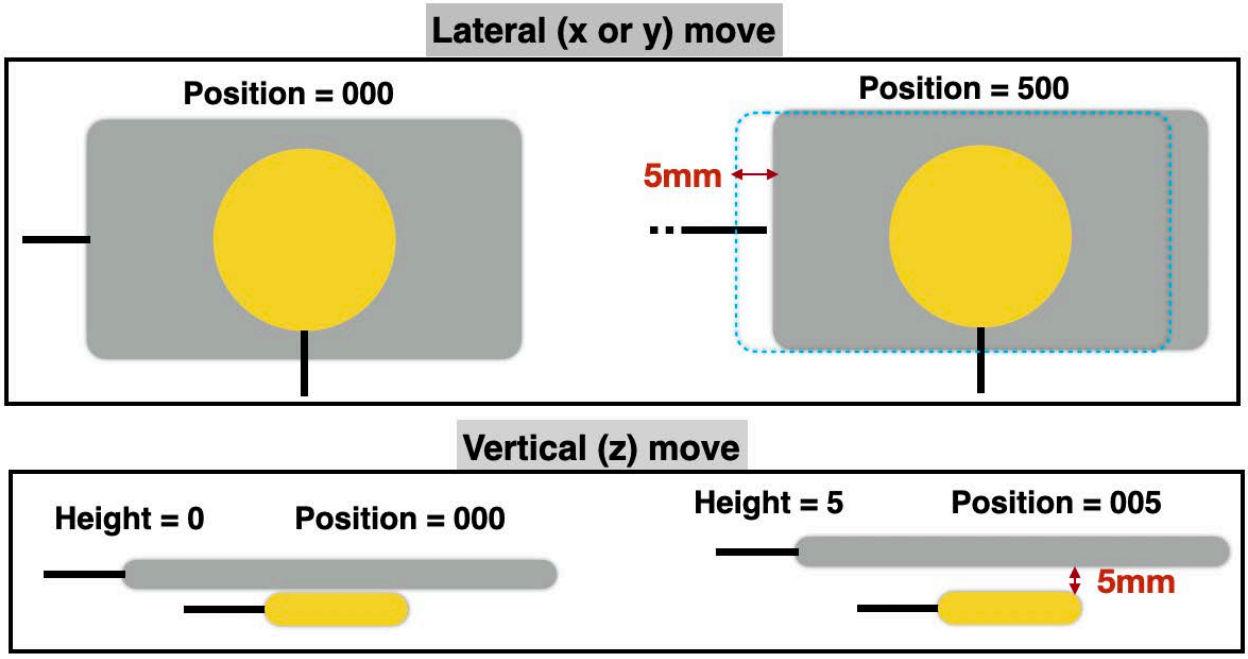

The misalignment and/or separation can change H-field's intensity and spatial distribution. Hence, several different misalignment and separation cases were selected and investigated to determine the worst-case scenario (i.e., highest H-field). After simulating these cases, some will be selected and measured and used to benchmark the accuracy of the simulation model. Finally, worst cases will be selected for SAR simulation.

To this end, the simulation and measurement results are compared for the phone and puck side below. The target power shows the maximum deliverable power per each case. For example, to be able to deliver a maximum power of 15 W to the phone, the maximum offset is found to be either 3 mm radially on z = 0 mm plane, or 2 mm radially on z = 2 mm plane.

For each side, the H-field probe is in contact with the DUT, scanning an area of 152 by 152 mm^2 with a step size of 3 mm. The maximum RMS H-field is reported in the tables.

There is a good correlation between the simulation and measurement results. Also, as tables show, for aligned cases (i.e., zero lateral move), the phone side shows relatively more radiation. This is mainly because the metallic housing of the puck preforms as a good shield. While when there is a lateral misalignment, fields can leak from the sides and the H-field on the puck side becomes more noticeable.

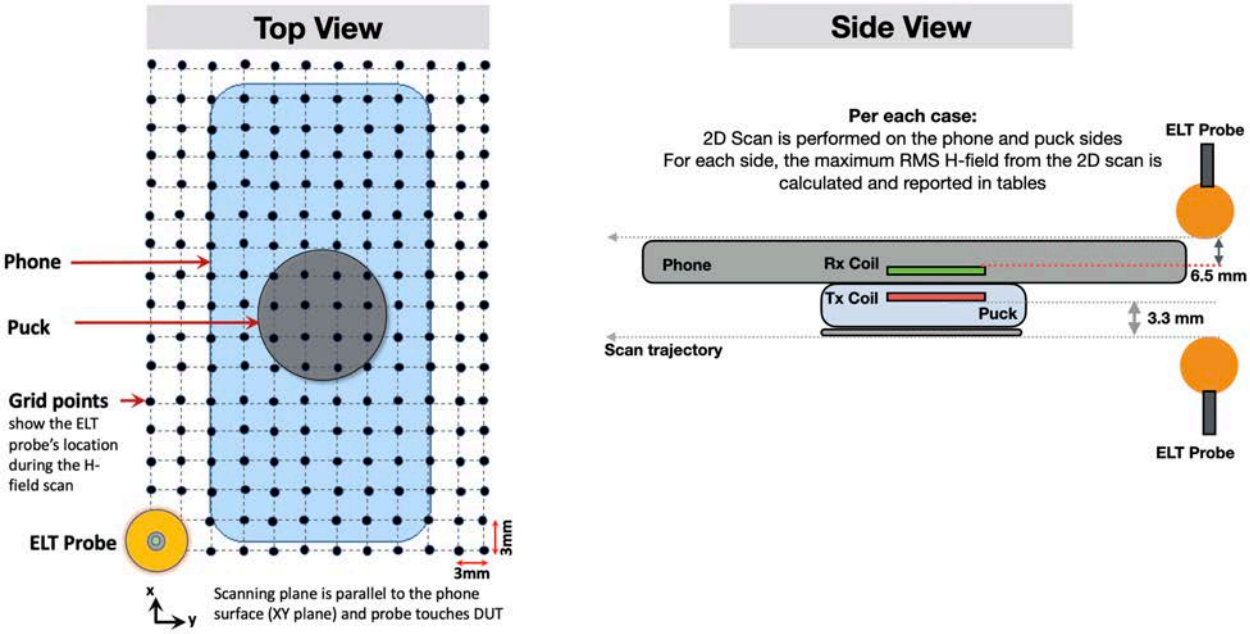

Phone Side RMS H-field (A/m)

Phone's Relative Move (X,Y,Z) from Alignment	Target Power	Simulation	Measurement
(0,0,0)	15	1.2	1.0
(0,0,1)	15	1.43	1.19
(0,0,2)	15	1.67	1.27
(0,0,3)	15	1.89	1.52
(0,0,4)	7.5	1.71	1.0
(0,0,5)	7.5	2.09	1.39
(2,0,2)	15	1.18	1.38
(2,0,3)	15	1.79	1.52
(3,0,3)	7.5	1.64	1.02
(4,0,3)	7.5	1.04	N/A
(4,0,4)	7.5	1.89	1.31
(5,0,0)	7.5	1.25	0.73
(5,0,5)	3.5	1.99	N/A
(7,0,0)	3.5	1.85	N/A

Puck Side RMS H-field (A/m)

Phone's Relative Move (X,Y,Z) from Alignment	Target Power	Simulation	Measurement
(0,0,0)	15	0.33	0.32
(0,0,1)	15	0.40	0.42
(0,0,2)	15	0.44	0.45
(0,0,3)	15	0.47	0.43
(0,0,4)	7.5	0.35	0.58
(0,0,5)	7.5	0.40	0.53
(2,0,2)	15	1.82	1.03
(2,0,3)	15	1.81	1.22
(3,0,3)	7.5	2.54	1.96
(4,0,3)	7.5	3.46	N/A
(4,0,4)	7.5	3.87	2.64
(5,0,0)	7.5	2.20	1.17
(5,0,5)	3.5	4.54	N/A
(7,0,0)	3.5	3.62	N/A

*N/A= Not Available: To save measurement time, only selected number of cases were measured.

To further validate the simulation model, one of the cases with the highest H-field (e.g., Case 404-Puck side) was selected and H-field correlation is performed at a vertical distance from back of the puck. The simulation and measurement curves are compared, below. There is a good correlation between the measurement and simulation curves. At distances very close to the DUT, simulation is always more conservative than measurement. For this specific DUT, H-field levels beyond 60 mm are below the noise floor, therefore, measured values remain flat while simulated values continue to decrease.

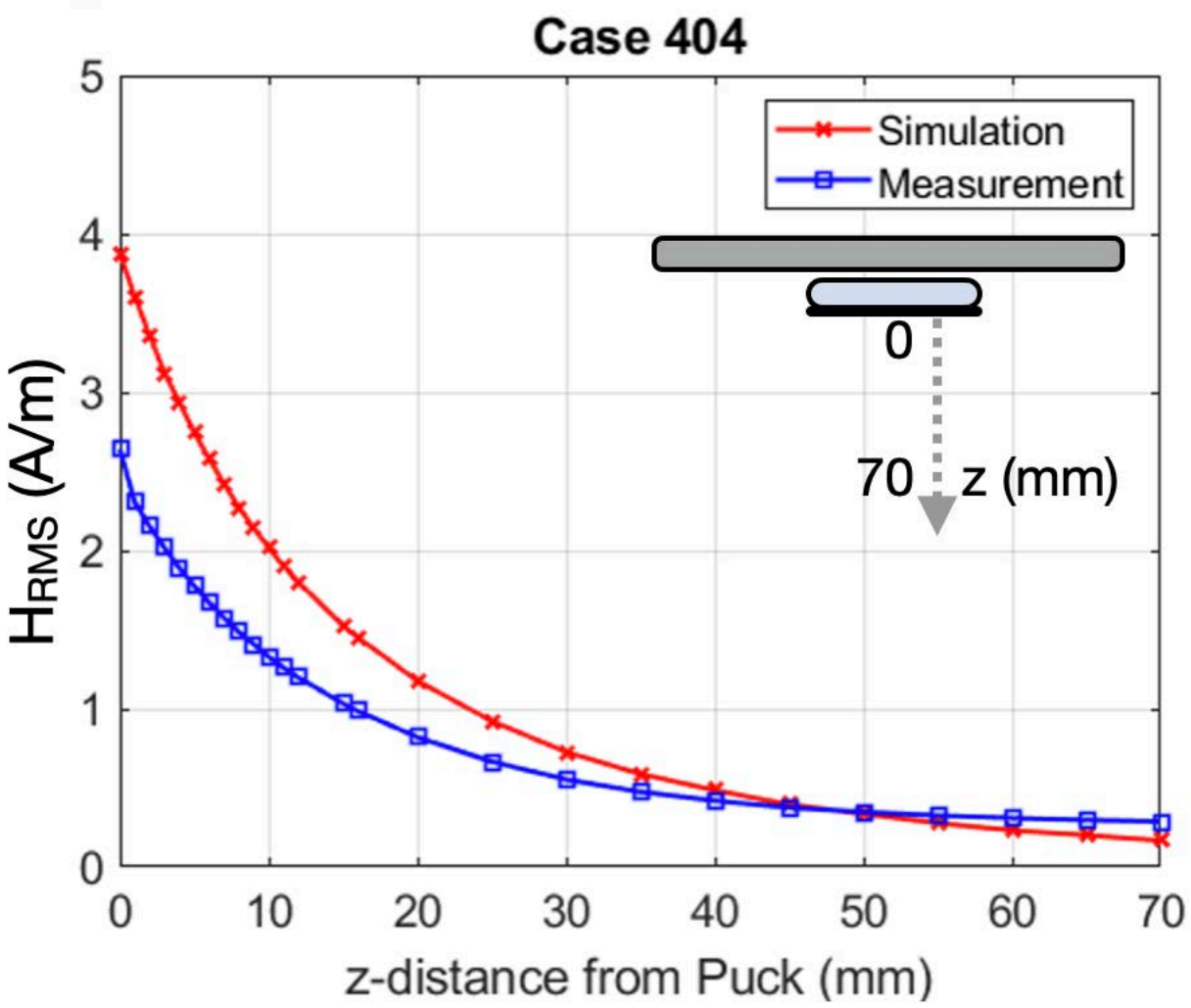

6 SAR Simulations

With correlation demonstrated between measurements and simulations, the same model is then used for SAR calculations with a phantom added in contact with the DUT. The simulations are computed on a 96 core CPU server with an available RAM of 4 Terabytes. For each simulation, the model run takes approximately 10 hours to complete.

The following steps are used for accurate SAR calculations:

1) Elliptical phantom used in body exposure measurements is commercially available from SPEAG: Outer Dimensions of 600 mm x 400 mm x 150 mm.
2) Homogeneous tissue material is used as liquid for the operating frequency.
3) Power loss in phantom is calculated.
4) Divide power loss by mass density to calculate SAR.

$$SAR = \frac{P_l}{\rho}$$

$$P_l = \text{Power loss density}$$

$$\rho = \text{Mass density}$$

5) Point SAR is averaged over 1g or 10g tissue.

Human Tissue Material Properties at 360 kHz:

The worst-case scenario has been identified to be when a user is holding the device in hand and taking a call or holding the phone on their body while charging. The electrical properties for body and hand layers are shown below. Since the SAR phantom is homogenous, using the layers' properties, the worst-case scenario is selected and applied for the phantom properties. Therefore, for the SAR simulations, the phantom that has conductivity of 0.5 and permittivity of 5016 at the 360 kHz operating frequency is used.

Electrical Properties:

Based on our research below are ε_r and σ values used for body layers:

Tissue	Thickness (mm)	Permittivity	Conductivity (S/m)
Skin	3	5016	0.16
Muscle	9	4666	0.5
Bone	20	1414	0.165
Worst case	100	5016	0.5

Based on our research below are ε_r and σ values used for hand layers:

Tissue	Thickness (mm)	Permittivity	Conductivity (S/m)
Skin	2	5016	0.16
Muscle	2	4666	0.5
Bone	15	1414	0.165
Worst case	100	5016	0.5

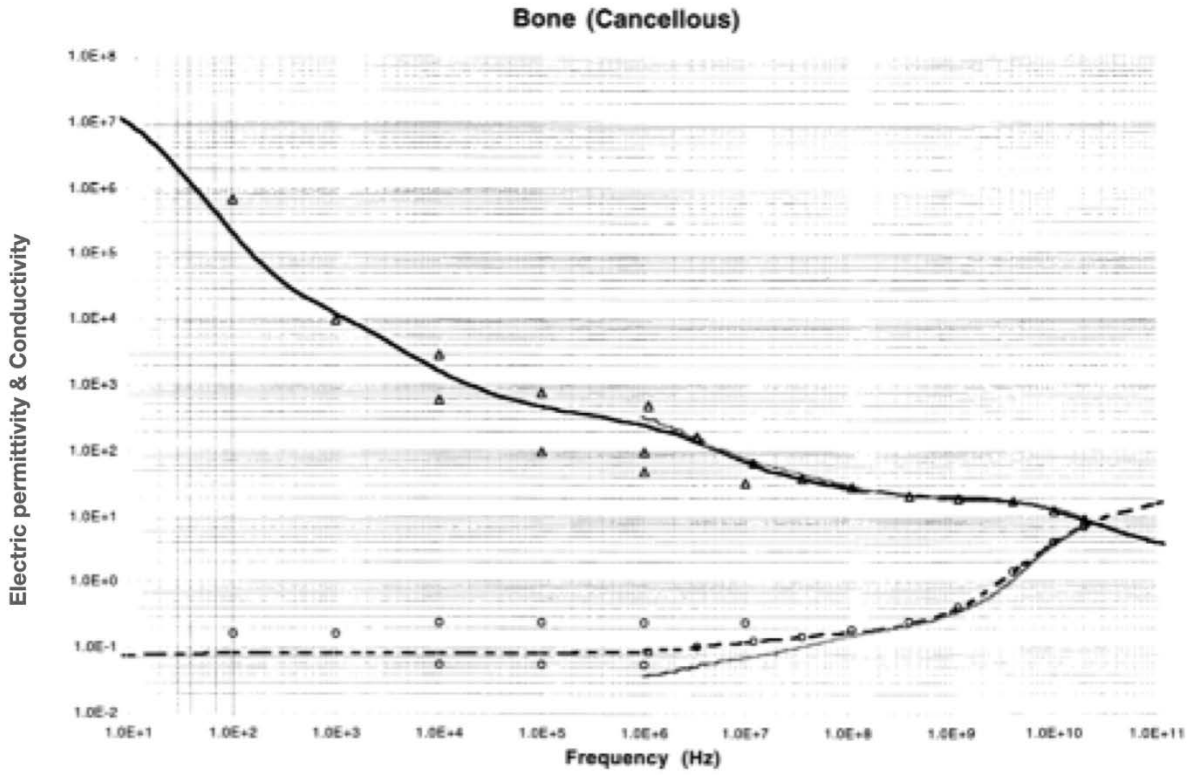
Bone (Cancellous)
Electric permittivity & Conductivity
1.0E+8
1.0E+7
1.0E+6
1.0E+5
1.0E+4
1.0E+3
1.0E+2
1.0E+1
1.0E+0
1.0E-1
1.0E-2
1.0E+1
1.0E+2
1.0E+3
1.0E+4
1.0E+5
1.0E+6
1.0E+7
1.0E+8
1.0E+9
1.0E+10
1.0E+11
Frequency (Hz)

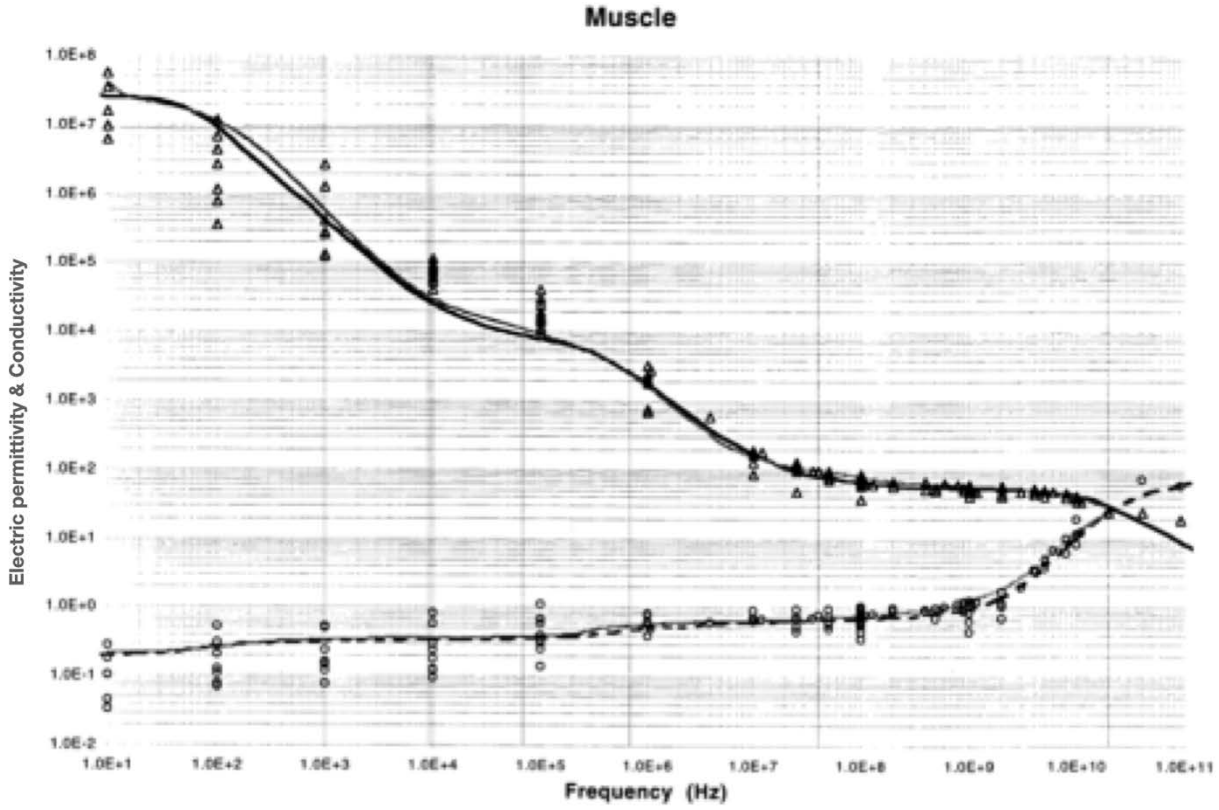
Muscle
Electric permittivity & Conductivity
1.0E+8
1.0E+7
1.0E+6
1.0E+5
1.0E+4
1.0E+3
1.0E+2
1.0E+1
1.0E+0
1.0E-1
1.0E-2
1.0E+1
1.0E+2
1.0E+3
1.0E+4
1.0E+5
1.0E+6
1.0E+7
1.0E+8
1.0E+9
1.0E+10
1.0E+11
Frequency (Hz)

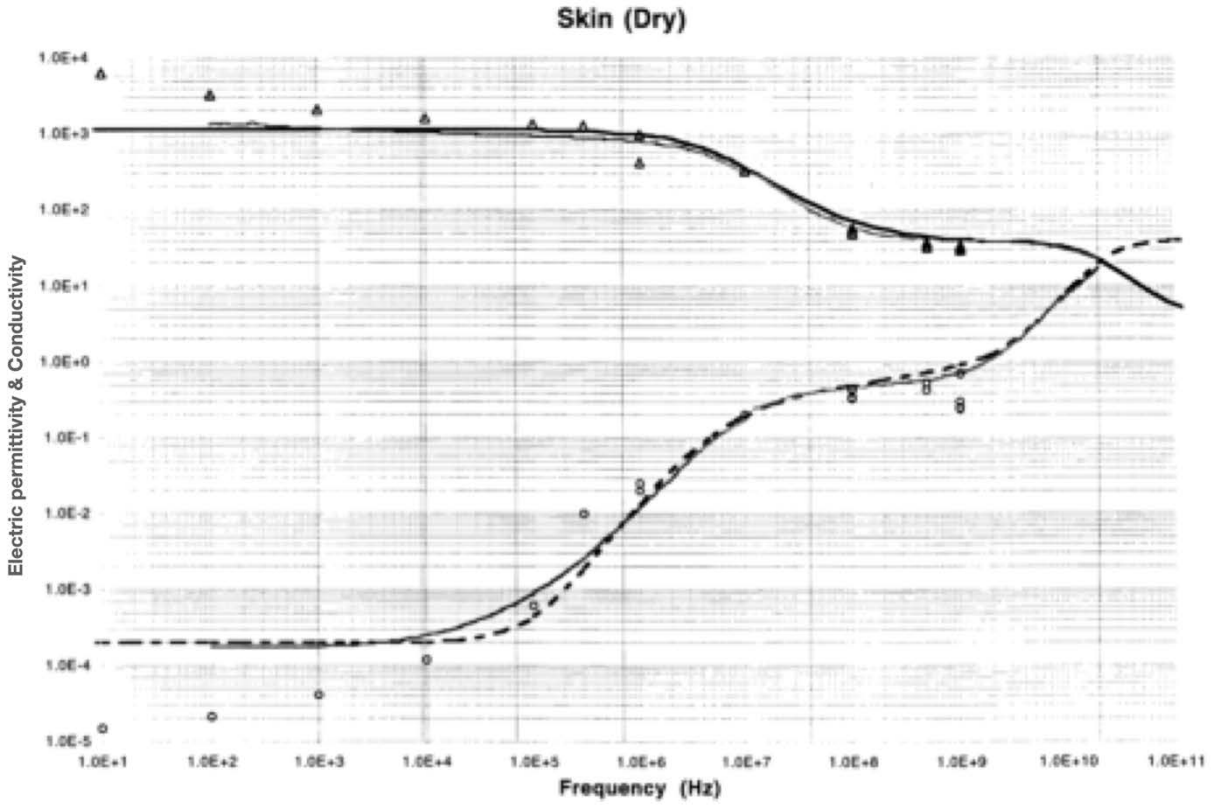

Mesh Adaptation:

HFSS adapts the mesh based on field strength. It is important to ensure the mesh is refined to capture SAR accurately. This can be done by using adaptive meshing available in HFSS.

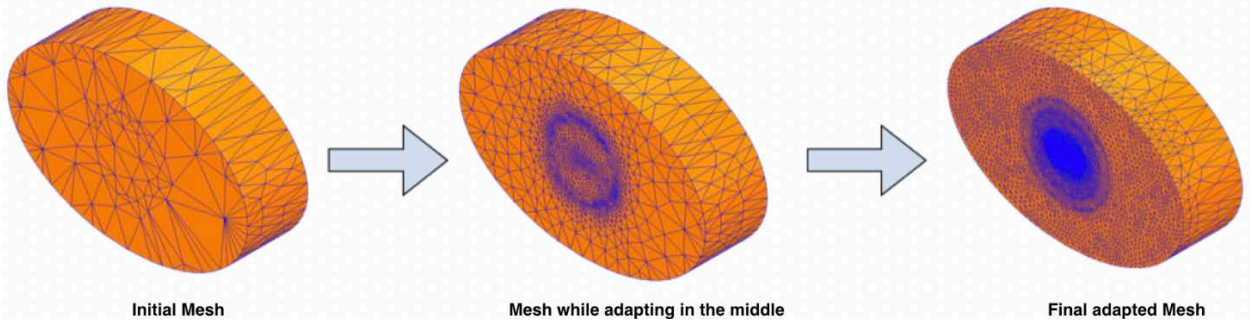

SAR Results:

Using the H-field simulation and measurement tables, two exposure cases were selected for SAR investigation. Considering that the phantom can be in contact with the phone or puck, there is a total of four scenarios.

> **Exposure Case 000 (a):** Nominal configuration with perfect alignment and phantom placed above the receiving unit.

Exposure Case 000(b): Nominal configuration with perfect alignment and phantom placed below the transmitting unit.
Exposure Case 505 (a): Misaligned configuration with the worst-case alignment and phantom placed above the receiving unit.
Exposure Case 505 (b): Misaligned configuration with the worst-case alignment and phantom placed below the transmitting unit.

In addition, two unrealistic cases where the puck is in direct contact with the phantom are investigated. Worth mentioning that these cases do not happen in real-life applications.

Unrealistic (Theoretical) Exposure Case 1(a): Unrealistic worst-case configuration with receiving unit absent and phantom placed above the transmitting unit.
Unrealistic (Theoretical) Exposure Case 1(b): Unrealistic worst-case configuration with receiving unit absent and phantom placed below the transmitting unit.

For all the exposure cases, dielectric properties (conductivity and permittivity) used for the phantoms are fixed as (permittivity: 5016, conductivity: 0.5). The coil properties are also fixed, transmitting coil with 11 turns and measures 7.5 uH nominally in free air. The receiver coil consists of 13 turns and measures 9.06 uH nominally in free air. Both coils are wound spirally.
The following outputs are calculated and reported in the Table:

a. Peak spatial 1-g average SAR in tissue.
b. Peak spatially averaged electric field in tissue. Electric field is spatially averaged in a contiguous tissue volume of 2 mm x 2 mm x 2 mm.

The simulation results for the four exposure cases are listed in the table below.

Exposure Case	Description	Peak Spatial Average SAR, [W/Kg] Averaged over 1 gram	Peak Spatial Avg E, [V/m] Averaged over 2x2x2 mm^3
Case 000 (a)		0.0000021	0.20
Case 000 (b)		0.00000113	0.107
Case 505 (a)	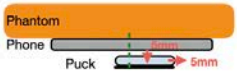	0.000008	0.37
Case 505 (b)	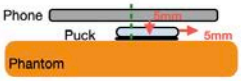	0.00020	0.83

Also, the simulation results for the two unrealistic (theoretical) exposure cases are listed in the table below.

Exposure Case	Description	Peak Spatial Average SAR, [W/Kg] Averaged over 1gram	Peak Spatial Avg E, [V/m] Averaged over 2x2x2 mm^3
Unrealistic (theoretical) Case 1(a)		0.1236	37.45
Unrealistic (theoretical) Case 1(b)		0.000049	0.45

SAR plot is presented for Case505(b). The peak spatial 1-gram average SAR is **0.0002 W/kg**.

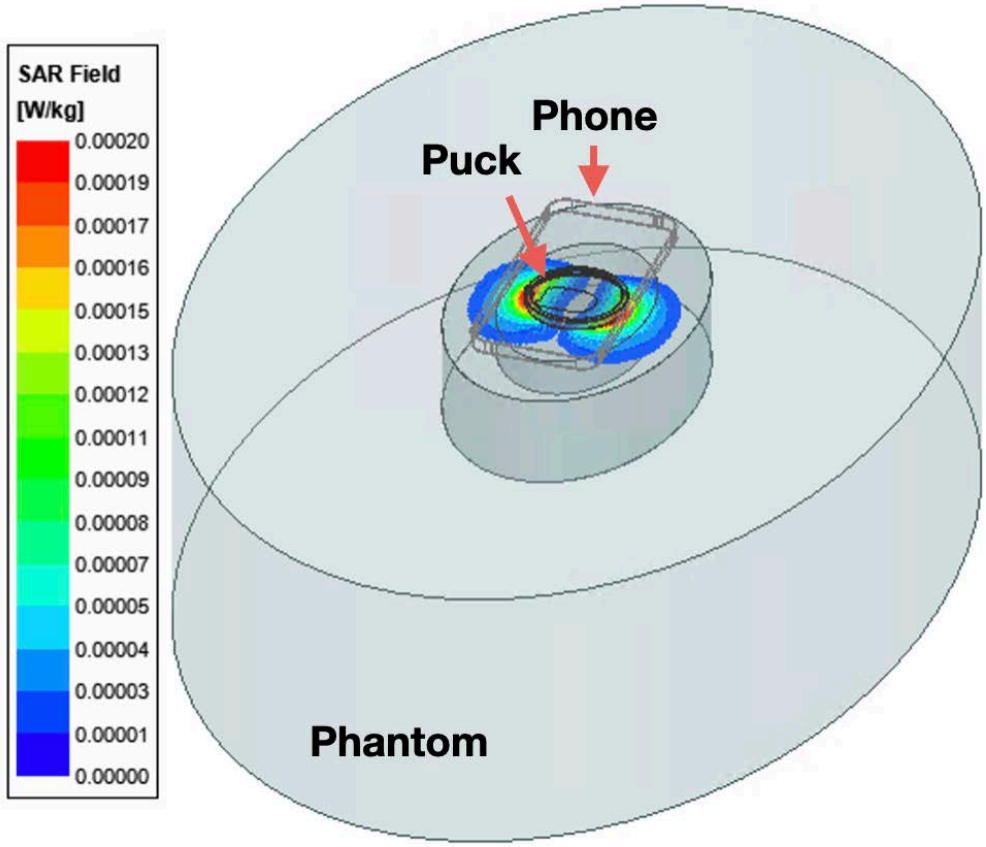

The cut view is also presented below.

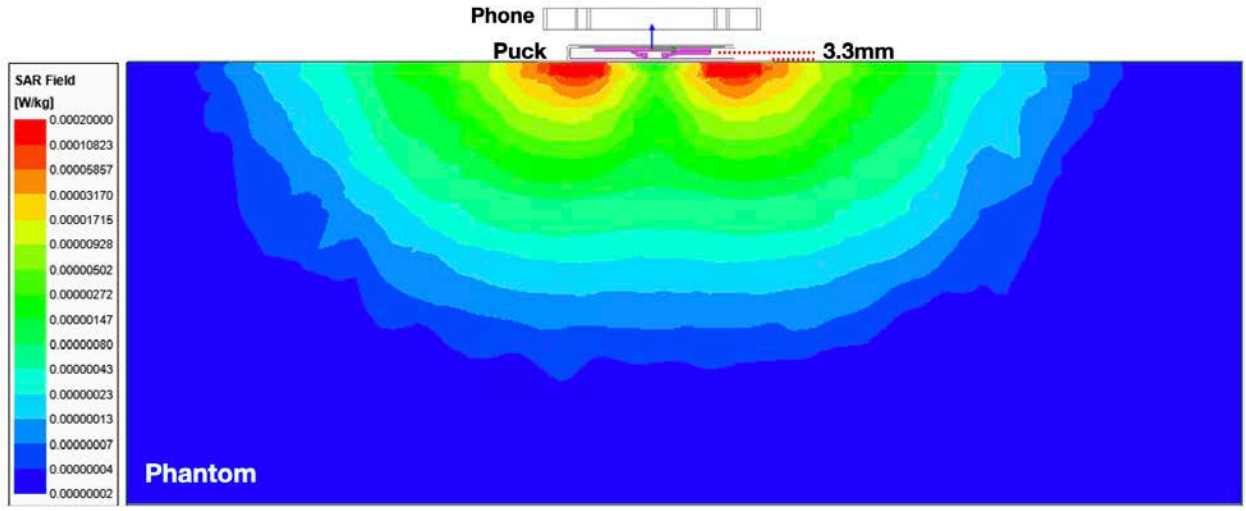

For the unrealistic (theoretical) Case 1(a), the spatial average 1-gram SAR is presented below.

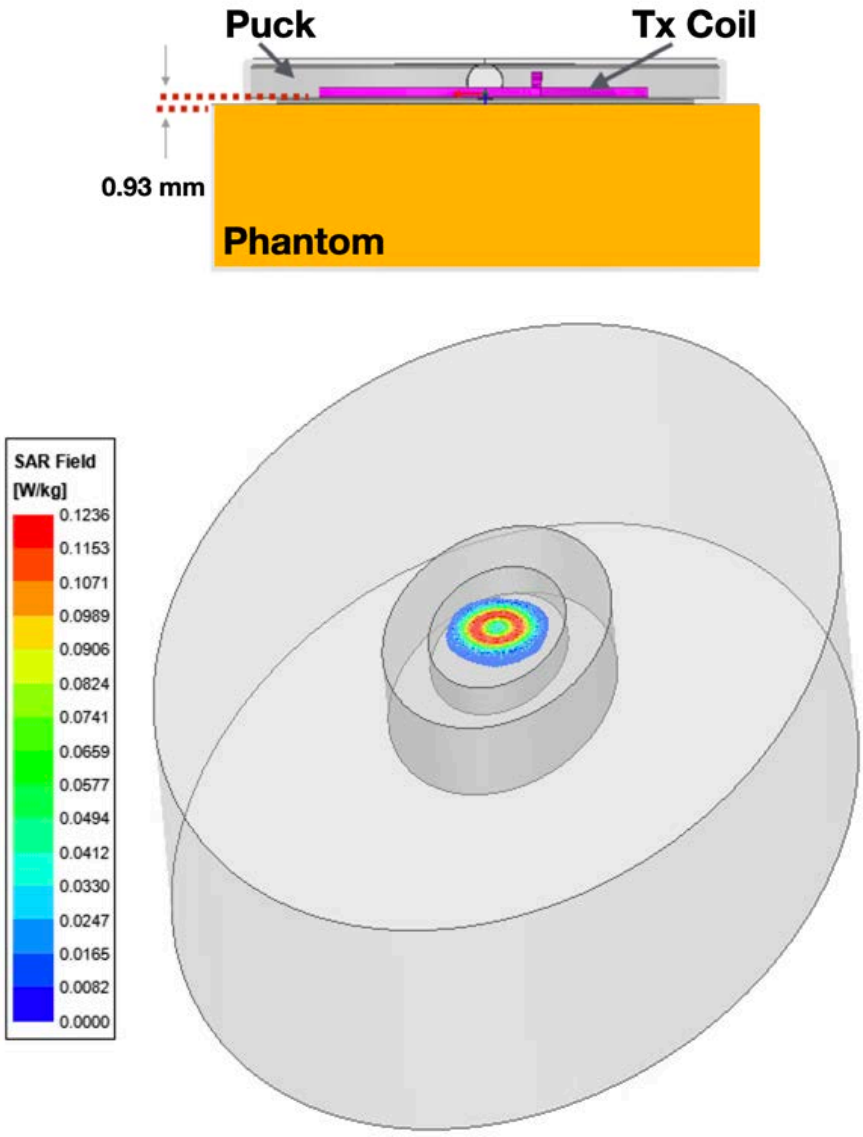

The cut view is also presented below.

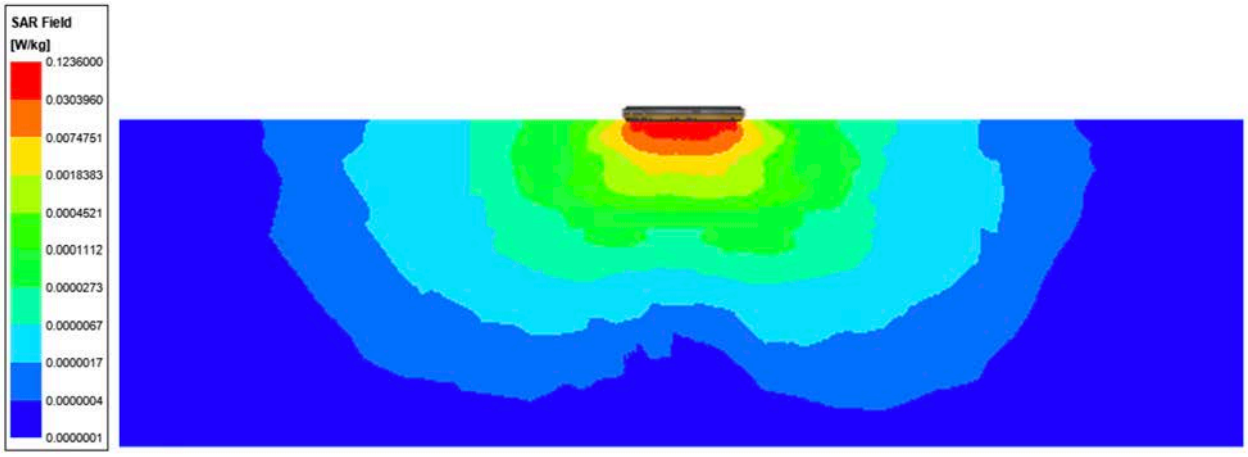

To show how the peak value would compare to the maximum allowable SAR limit, we manually changed the plotting scale and set the highest value to 1.6 W/kg. As it can be seen below, the peak spatial SAR is well below the limit.

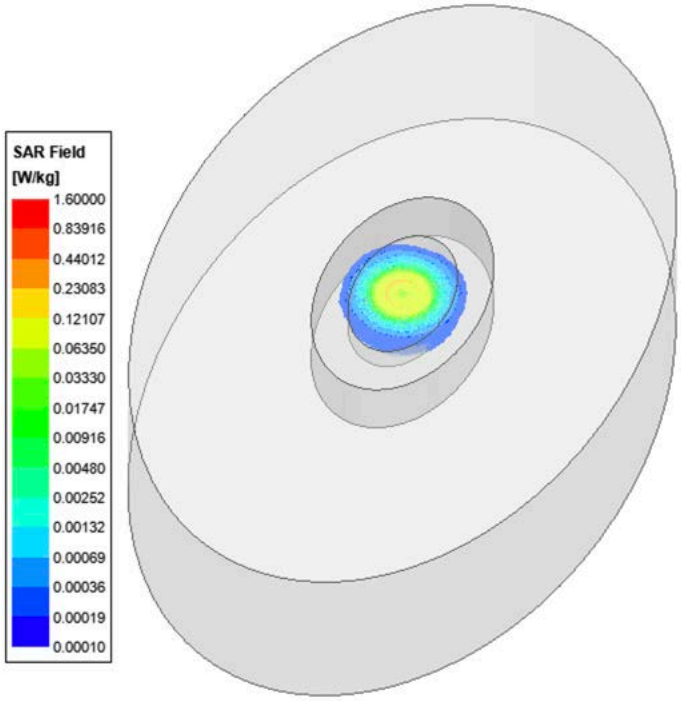

Note: The colormap scale is manually adjusted, the peak value of the spatial average SAR is only 0.1236 W/Kg.

Moreover, the E-field distribution inside the phantom for the Case1(a) is shown below. Note that the value reported in table was averaged over a cube of 2 mm x 2 mm x 2 mm and that explains why the value is lower than the Peak E-field in this plot.

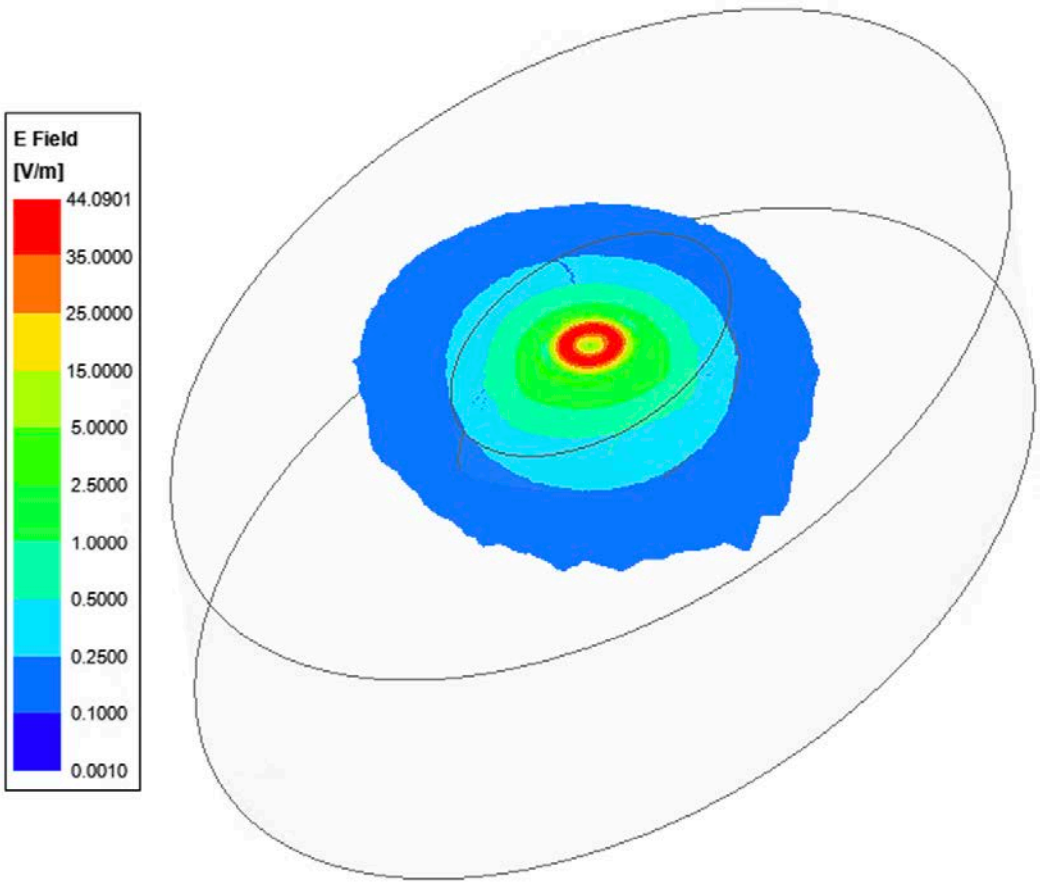
E Field
[V/m]
44.0901
35.0000
25.0000
15.0000
5.0000
2.5000
1.0000
0.5000
0.2500
0.1000
0.0010

7 Summary

Based upon the above results, the accuracy of the SAR simulations is demonstrated by correlating H-field measurements to simulations. The validity of using this modeling and SAR computational method hence is established. For the nominal case where the puck and the phone are aligned without any vertical separation, the highest peak spatial 1-gram average SAR is 0.0000021 W/Kg and the highest peak spatial average E field (i.e., averaged over a cube of 2mmx2mmx2mm) is 0.2 V/m.

8 Annex A: Specific Information for SAR Computational Modelling

1) Computation Resources

The model is simulated on a 96 core CPU server with an available RAM of 4 Terabytes. Each model simulation takes around 10 hours to complete. Based on the simulation profile, the minimum resources needed to finish these simulations will be approximately 8 core CPU with 512 GB of RAM. Using the minimum requirements simulation will likely take more time than 12 hours.

2) Algorithm Implementation and Validation

This section is divided into two parts. The code performance validation provides methods to determine that the finite-element algorithm in HFSS has been implemented correctly and works accurately within the constraints due to the finite numerical accuracy. It further determines the quality of absorbing boundary conditions and certain parts of the post processing algorithms that are part of HFSS. The second part has few canonical benchmarks. All benchmarks can be compared to analytical solutions of the physical problem or its numerical representation. The methods characterize the implementation of the finite-element algorithm used by HFSS in a very general way. They are defined such that it is not possible to tune the implementation for a particular benchmark or application without improving the overall quality of the code.

2.1) Code Performance Validation

2.1.1) Propagation Homogeneous Medium

A straight rectangular waveguide with ports on both ends is well suited as a first test of an implementation of the Finite-Element Method used by HFSS. The waveguide has a width of 20 mm, a height of 10 mm and a length of 300 mm. The waveguide is filled homogeneously with a material which, in three separate simulations, shall assume the following properties:

i. $\varepsilon_r = 1$, $\sigma = 0$ S/m;
ii. $\varepsilon_r = 2$, $\sigma = 0$ S/m;
iii. $\mathrm{Re}(\varepsilon_r) = 2$, $\sigma = 0.2$ S/m.

To verify that the mesh used by HFSS is independent of orientation, the waveguide has been rotated so that it is not parallel with any principal coordinate plane (XY, XZ, YZ). The waveguide is driven in the TE10 mode at 10 GHz. Reported are the magnitudes of S21 and S11, as well as the values of the real and imaginary parts of the propagation constant γ. The table

below provides the reference values [B1], acceptable result criteria, as well as the simulated results.

Criteria for the Waveguide Evaluation

Re(ε_r)	1	2	2
σ	0	0	0.2
|S21| reference value	1	1	8.7 × 10-5
Criterion for |S21|	≥ 0.9999	≥ 0.9999	± 5 × 10-6
|S21| simulated results	1	1	8.7 × 10-5
|S11| reference value	0	0	0
Criterion for |S11|	≤ 0.003	≤ 0.003	≤ 0.003
|S11| simulated results	0	0	0
Re(γ) reference value	0	0	31.17 m^-1
Criterion for Re(γ)	± 0.1 m^-1	± 0.1 m^-1	± 2%
Re(γ) simulated results	0	0	31.17
Im(γ) reference value	138.75 m^-1	251.35 m^-1	253.28 m^-1
Criterion for Im(γ)	± 2%	± 2%	± 2%
Im(γ) simulated results	138.75	251.35	253.28

As is seen in the above table, HFSS easily meets the criteria for properly and accurately calculating the waveguide problem.

2.1.2) Planar Dielectric Boundary

In order to test the reflection of a plane wave by a dielectric boundary, a rectangular waveguide can again be used. It is well known that the TE10 mode can be thought of as a superposition of two plane waves [B1]. Each wave's direction of propagation makes an angle θ with the axis of the wave guide, given by

$$\cos^2\theta = 1 - (c/2af)^2 \quad (1)$$

where c is the speed of light, a is the width of the wave guide and f is the frequency. Assuming the axis of the waveguide is the Z axis and assuming the waveguide is filled with vacuum for Z > 0 and filled with dielectric 1 with complex relative permittivity ε_r for Z < 0, Fresnel reflection coefficients for the TE and the TM cases, defined as ratios of electric field strengths, are given by [B2]

$$R^{TE} = (k_{0,z} - k_{1,z}) / (k_{0,z} + k_{1,z}) \quad (2)$$

$$R^{TM} = (\varepsilon_r k_{0,z} - k_{1,z}) / (\varepsilon_r k_{0,z} + k_{1,z}) \quad (3)$$

where $k_{0,z}$ and $k_{1,z}$ denote the z component of the propagation vector of the plane wave in vacuum and in the dielectric, respectively. They can be evaluated through

$$k_{0,z} = k_0 \cos\theta \quad (4)$$
$$k_{1,z} = k_0 \sqrt{(\varepsilon_r - \sin^2\theta)} \quad (5)$$

Finally, ε_r is complex and is given by

$$\varepsilon_r = \mathrm{Re}(\varepsilon_r) - j\sigma/(2\pi f\varepsilon_0) \quad (6)$$

where $\mathrm{Re}(\varepsilon_r)$ denotes the real part of the relative permittivity, σ is the conductivity of the medium, and ε_0 is free space permittivity 8.85e-12 F/m.

For this test, a 20 mm × 10 mm waveguide with a length of 60 mm, as shown below, was created. The top half was filled with vacuum and the bottom half with dielectric.

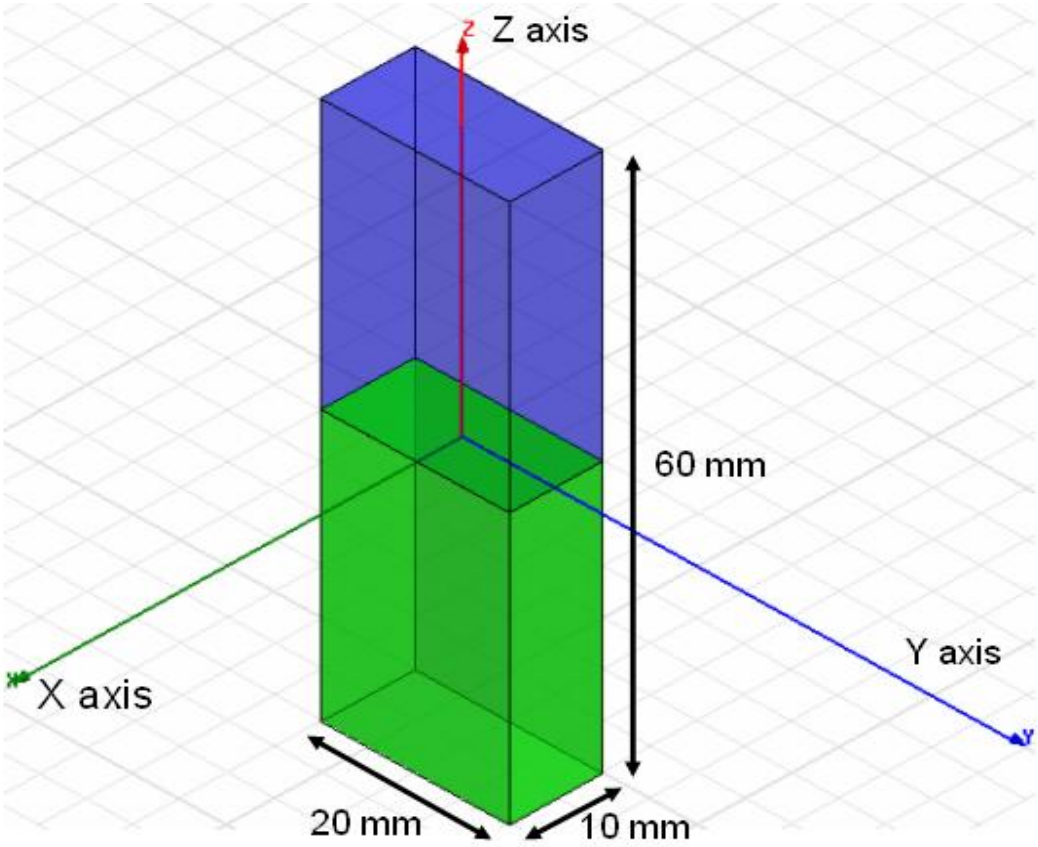

Waveguide Filled Half with Vacuum and Half with Dielectric

In one copy of the model, all side walls were lossless metal, such that the dominant mode is the TE_{10} mode with propagation constant 138.75 m^-1 at 10 GHz and represents the TE case in the reflection analysis. In the other copy of the model, the side walls that are parallel to the YZ plane were perfect magnetic conductors while the other walls were perfect electric conductors, such that the second mode (after a TEM mode which won't be used in this test) has propagation constant 138.75 m^-1 at 10 GHz and represents the TM case in the reflection analysis.

Before simulation, the waveguides were rotated over an arbitrary angle such that no face is parallel with any coordinate plane. The waveguides were driven at 10 GHz in the proper mode. In doing so, it is good practice to calculate all propagating modes, but the coupling between modes is expected to be negligible. Simulations were run for the cases of lossless and lossy

dielectric as shown in the next table. For the HFSS to pass the test, according to IEC 62704-1, the results need to be within 2% of the analytical values.

Reflection at a Dielectric Interface

$Re(\varepsilon_r)$	σ (S/m)	RTE	RTE- Simulated	RTM	RTM - Simulated
4	0	0.4739	0.4739	0.1763	0.1763
4	0.2	0.4755	0.4755	0.1779	0.1779
4	1	0.5105	0.5105	0.2121	0.2121

As can be seen from the data, HFSS produces results identical to the analytical values.

2.2) Canonical Benchmarks

The results for few low frequency benchmarks are summarized below. These benchmarks were used to validate the accuracy of the tool at low frequencies:

2.2.1) Dipole Antenna:

The following parameter were used in the dipole antenna to resonate at 400 kHz.

Dipole length: 375 meters
Feed gap: 2.5 meters
Dipole diameter: 5 meters

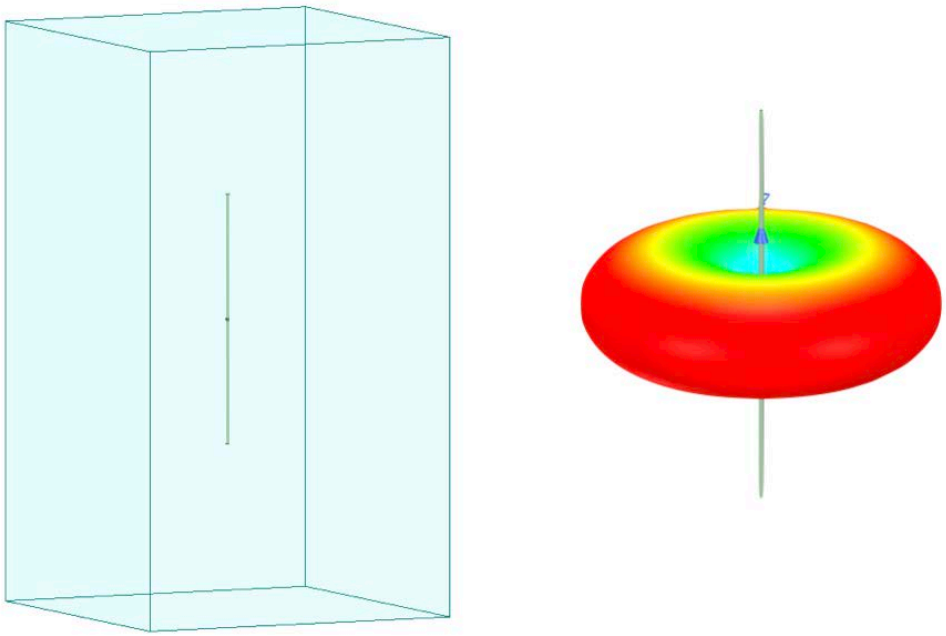

Dipole Antenna Model

IEC 62704-4 ED1 was referenced to compare the tables. Two computation methods were demonstrated as shown below to show the validity of the model.

Simulated Dipole Parameters

FEM Solver

Quantity	Simulation results	Tolerance	Satisfied?
Re(Z) at 400 KHz	**94.09**		
Im(Z) at 400 KHz	**55.62**		
Re(Z) at 320 KHz	**39.26**	$25\Omega < Re(Z) < 50\Omega$	Yes
Im(Z) at 320 KHz	**-90.52**	$-50\Omega < Im(Z) < -100\Omega$	Yes
Re(Z) at 360 KHz	**59.58**	$50\Omega < Re(Z) < 75\Omega$	Yes
Im(Z) at 360 KHz	**-18.30**	$-25\Omega < Im(Z) < 0\Omega$	Yes
Frequency for Im(Z) =0	**370**	$360MHz < f < 380MHz$	Yes
Maximum power budget error	**0.3**	$< 5\,\%$	Yes

MoM Solver

Quantity	Simulation results	Tolerance	Satisfied?
Re(Z) at 400 KHz	**98.45**		
Im(Z) at 400 KHz	**53.57**		
Re(Z) at 320 KHz	**43.31**	$25\Omega < Re(Z) < 50\Omega$	Yes
Im(Z) at 320 KHz	**-90.55**	$-50\Omega < Im(Z) < -100\Omega$	Yes
Re(Z) at 360 KHz	**65.03**	$50\Omega < Re(Z) < 75\Omega$	Yes
Im(Z) at 360 KHz	**-18.59**	$-25\Omega < Im(Z) < 0\Omega$	Yes
Frequency for Im(Z) =0	**370**	$360MHz < f < 380MHz$	Yes
Maximum power budget error	**0.02**	$< 5\,\%$	Yes

2.2.2) Toroid Inductor:

The parameters of the toroid were chosen to be

N = 20
A = 6.35e-4 m^2
R = 0.0263 m
ur = 64

The formula below gave an inductance of 139 uH. The model created in HFSS gave an inductance of 139.9 uH.

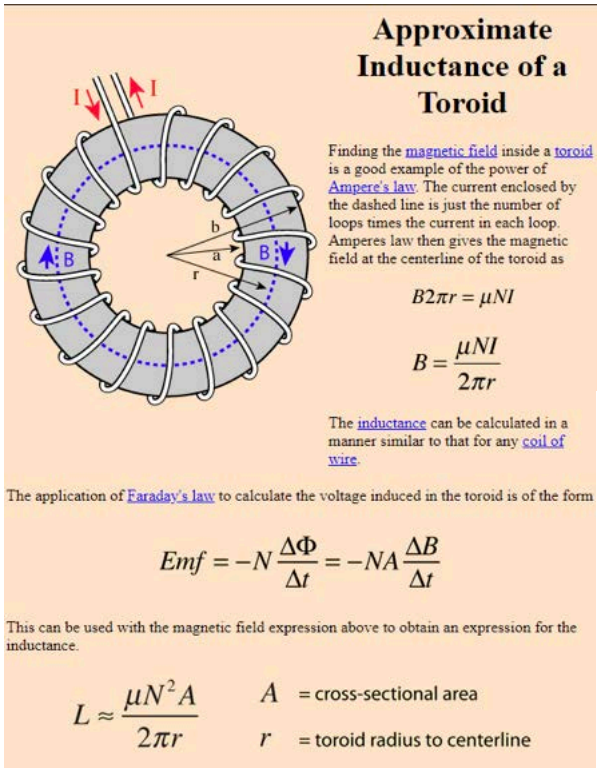

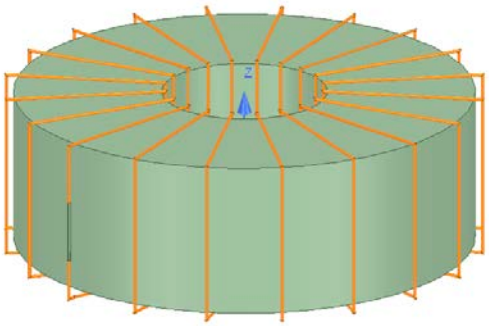

Toroid Model

2.2.3) Circular Coil Parallel to a Flat, Homogeneous Phantom.:

The following benchmark is implemented using Equations 1-4 of the referenced Chen et al. (2014) paper and also matches Figure 6 therein scaled to 10 coil turns.

Below is the coil and phantom parameters:

Coil Diameter: 50 mm
Number of Turns: 10
RMS Current: 0.707 A (peak current = 1 A)
Frequency: 100 kHz
Coil-to-Body Distance: 5 mm
Tissue Conductivity: 0.05 S/m
Tissue Permittivity: 1120

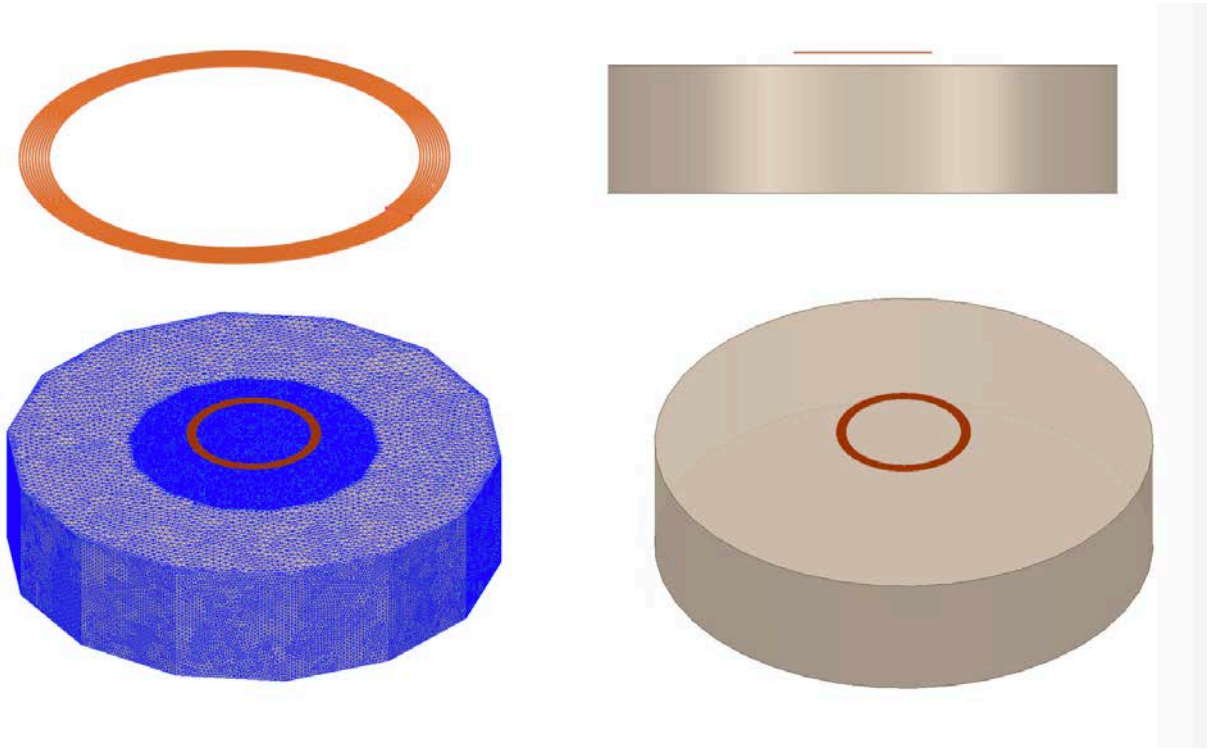

Current Loop in Front of a Cuboid

The simulated spatial peak RMS electric field in tissue is 1.51 V/m compared to the analytical value of 1.47 V/m.

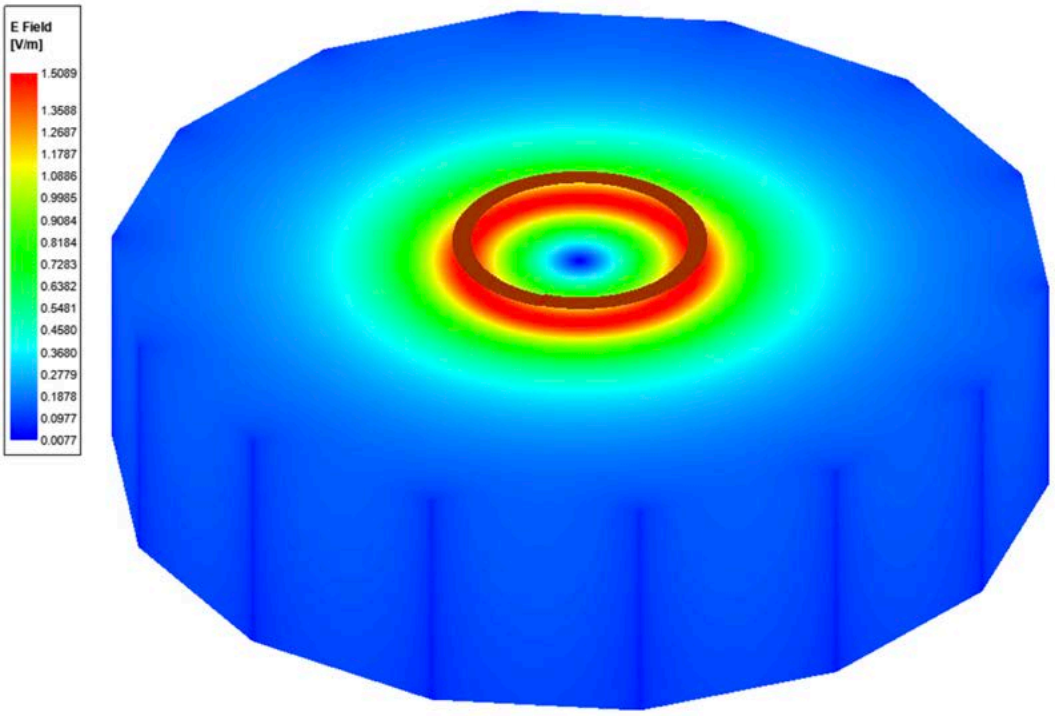

Current Density Plot

3) Computational Peak SAR from Peak Components & 1-g Averaged SAR Procedure

The calculation method for SAR follows IEEE P1528.4. Once the solver calculated the S-Parameter results, different coils can be driven and the result from the S-Parameter calculation is automatically scaled to the driving current of the coils. This result combination provides the correctly scaled power loss density in the phantom. The SAR calculation computes the local SAR first using electric field and conducting current:

$$SAR = \vec{E} \bullet \vec{J}_{conj}/(2\rho)$$

Afterwards the local SAR is averaged over a specific mass, usually 1g or 10g. As described in [IEEE P1528.4] the mass averaging is done by mapping the results to a structured hexahedral grid and afterwards the averaging scheme for FDTD per [IEEE P1528.4] is applied. The SAR calculation on the hexahedral grid is compliant with IEC 62704-1.

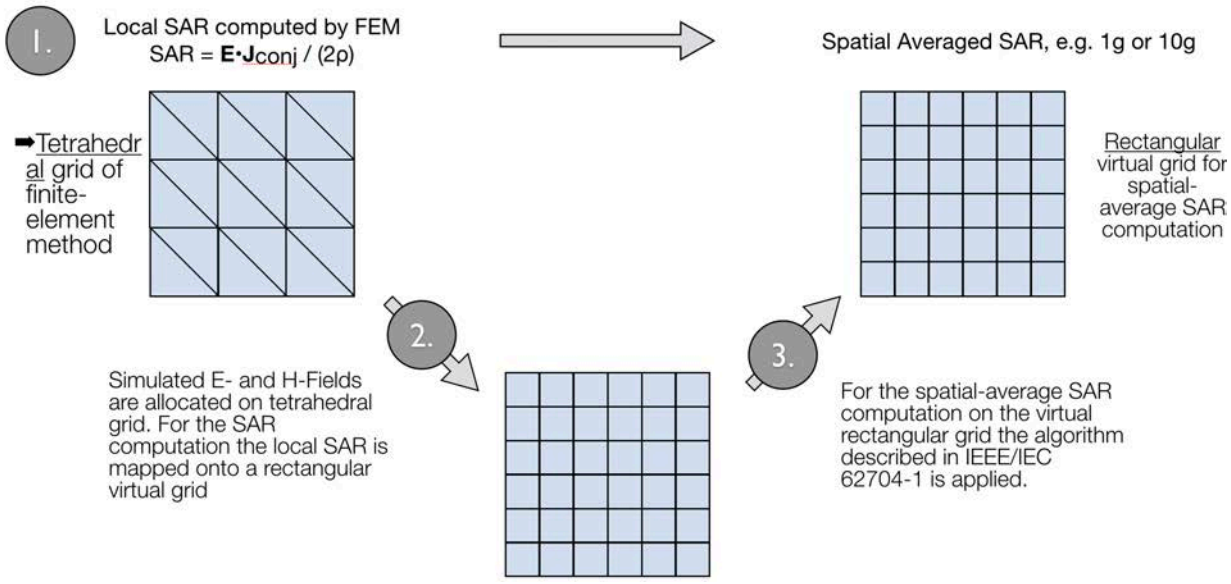

IEEE P1528.4 SAR Computation

4) Total Computational Uncertainty

Below is a table summarizing the budget of the uncertainty contributions of the numerical algorithm and of the rendering of the simulation-setup. The table was filled using the IEC 62704-4 ED1.

For the simulations, the extreme case where the phantom is placed directly in front of the puck is considered. Among all of the investigated conditions, the positioning generated the highest uncertainty. This mainly roots from the fact that based on the instruction in 7.2.2 subclause, a 0.71 mm air gap was inserted between the puck and the phantom, leading to a large discontinuity. Therefore, the SAR value of the model with displaced phantom changed compared to the baseline (contact) case. Worth mentioning that since ANSYS HFSS uses a sophisticated adaptive meshing technique enhanced with an advanced initial meshing technology, the

generated mesh can conform to complex geometries, well. This mitigates the artificial gap that a poor mesh could introduce between the touching objects.

Uncertainty Table

a	b	d	e	g
Uncertainty component	**Subclause**	**Probability distribution**	**Divisor f(d, h)**	**Uncertainty %**
Positioning	7.2.2	R	1,73	**19**
Mesh resolution	7.2.3	N	1	**0.01**
ABC	7.2.4	N	1	**0.08**
Power budget	7.2.5	N	1	**0.0**
Convergence	7.2.6	R	1,73	**0.01**
Phantom dielectrics	7.2.7	R	1,73	**0**
Combined standard uncertainty (k = 1)				**19.2**

Below is a table summarizing the budget of the uncertainty of the developed model of the DUT. The table was filled using the IEC 62704-4 ED1.

Two probe separation was considered, 0 mm and 30 mm. The uncertainty at 0 mm is much higher because of the probe coupling to DUT.

Probe in contact (case with highest measured H-field, Case404-Puck side):

a	b	d	e	g
Uncertainty component	**Subclause**	**Probability distribution**	**Divisor f(d, h)**	**Uncertainty %**
Uncertainty of the DUT model (based on near field distribution)	7.2.2	N	1	**46**
Uncertainty of the measurement equipment and procedure	7.2.3	N	1	**4**
Combined standard uncertainty (k = 1)				**50**

Probe 30 mm away (Case 404-Puck side):

a	b	d	e	g
Uncertainty component	**Subclause**	**Probability distribution**	**Divisor f(d, h)**	**Uncertainty %**
Uncertainty of the DUT model (based on near field distribution)	7.2.2	N	1	**27**
Uncertainty of the measurement equipment and procedure	7.2.3	N	1	**4**
Combined standard uncertainty (k = 1)				**31**

SAR calculations are also performed using specific standard anthropomorphic model (SAM) for the use-case of the WPT device described in this report. The use-case for the WPT device is shown in below. SAM accurate model with appropriate frequency-dependent SAM tissue dielectric properties are used in the simulation [Ref. 3]. The average SAR is calculated for the worst-case scenario with peak current of 3A as the input excitation source for the coil. The average SAR value is 0.0057 W/Kg. The SAR values from anatomical model is much lower than worst case scenario used in the main section, which only impacts the uncertainty calculation in the negative direction, making the presented data in section 6 always representing worst case numbers.

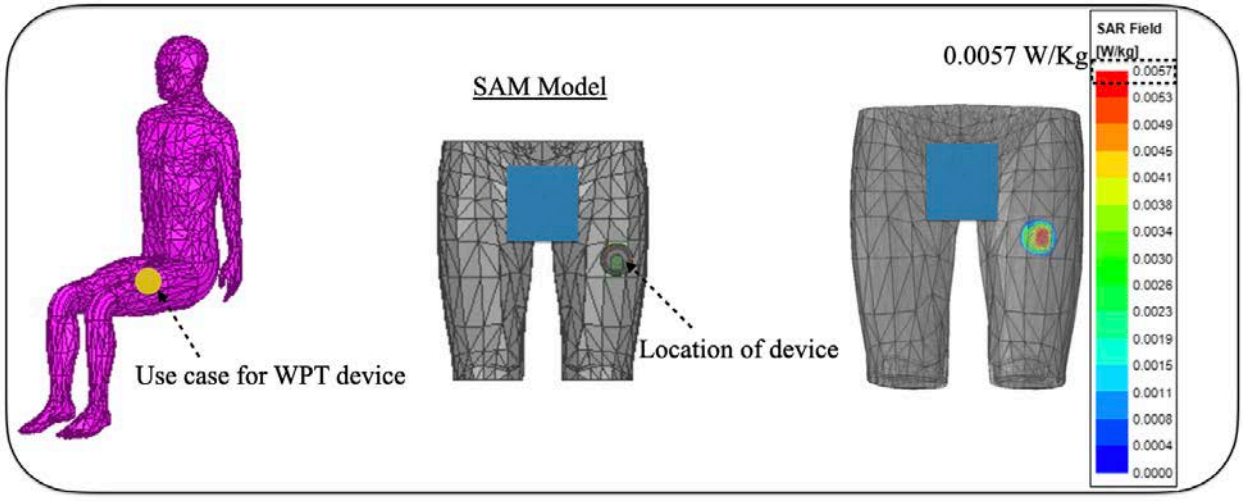

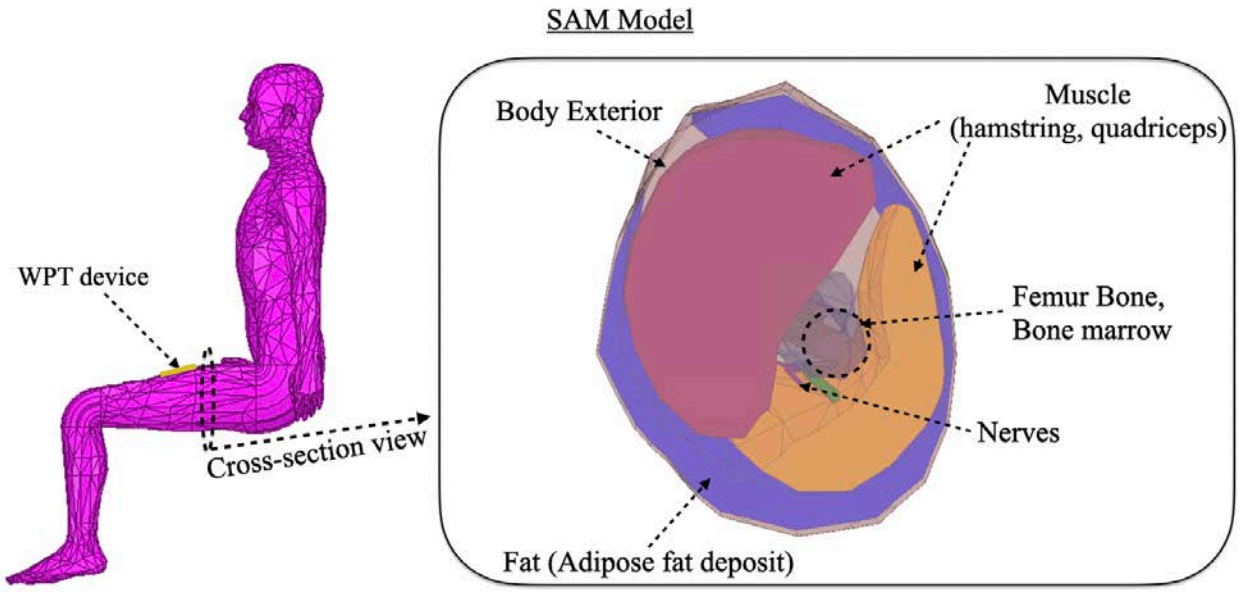
SAM Model
WPT device
Cross-section view
Body Exterior
Muscle
(hamstring, quadriceps)
Femur Bone,
Bone marrow
Nerves
Fat (Adipose fat deposit)

References:

1) The electrical conductivity of human cerebrospinal fluid at body temperature, S.B. Baumann ; D.R. Wozny ; S.K. Kelly ; F.M. Meno, IEEE Transactions on Biomedical Engineering (Volume: 44 , Issue: 3 , March 1997)
2) C.Gabriel, S.Gabriel and E.Corthout: The dielectric properties of biological tissues: I. Literature survey, Phys. Med. Biol. 41 (1996), 2231-2249.
3) S.Gabriel, R.W.Lau and C.Gabriel: The dielectric properties of biological tissues: II. Measurements in the frequency range 10 Hz to 20 GHz, Phys. Med. Biol. 41 (1996), 2251-2269.
4) S.Gabriel, R.W.Lau and C.Gabriel: The dielectric properties of biological tissues: III. Parametric models for the dielectric spectrum of tissues, Phys. Med. Biol. 41 (1996), 2271-2293.
5) https://itis.swiss/virtual-population/tissue-properties/database/thermal-conductivity/
6) http://hyperphysics.phy-astr.gsu.edu/hbase/magnetic/toroid.html
7) X. L. Chen et al., "Human Exposure to Close-Range Resonant Wireless Power Transfer Systems as a Function of Design Parameters," in IEEE Transactions on Electromagnetic Compatibility, vol. 56, no. 5, pp. 1027-1034, Oct. 2014.